

Magnetic data radial inversion for 3-D source geometry estimation

L.B. Vital^{1*}

¹ *Observatório Nacional, Gal. José Cristino, 77, São Cristóvão, Rio de Janeiro, 20921-400, Brazil*

Key words: Numerical solutions; Inverse theory; Magnetic anomalies.

* Observatório Ncional, ON

1 METHODOLOGY

1.1 Forward problem

Let \mathbf{d}^o be the observed data vector, whose i th element d_i^o , $i = 1, \dots, N$, is the total-field anomaly produced by a 3-D source (Fig. 1a) at the point (x_i, y_i, z_i) of a Cartesian coordinate system with x , y and z axes pointing to north, east and down, respectively. We assume that the direction of the total magnetization vector of the source is constant and known. We approximate the volume of the source by a set of L vertically juxtaposed 3-D prisms (Fig. 1b) by following the same approach of Oliveira Jr. et al. (2011) and Oliveira Jr. & Barbosa (2013). The depth to the top of the shallowest prism is defined by z_0 and m_0 is the constant total-magnetization intensity of all prisms. The horizontal cross-section of each prism is described by a polygon with a fixed number V of vertices equally spaced from 0° to 360° , which are described in polar coordinates referred to an internal origin O^k . The radii of the vertices $(r_j^k, j = 1, \dots, V, k = 1, \dots, L)$, the horizontal coordinates $(x_0^k$ and $y_0^k, k = 1, \dots, L)$ of the origins $O^k, k = 1, \dots, L$, and the depth extent dz of the L vertically stacked prisms (Fig. 1b) are arranged in a $M \times 1$ parameter vector \mathbf{p} , $M = L(V + 2) + 1$, given by

$$\mathbf{p} = \begin{bmatrix} \mathbf{r}^{1\top} & x_0^1 & y_0^1 & \dots & \mathbf{r}^{L\top} & x_0^L & y_0^L & dz \end{bmatrix}^\top, \quad (1)$$

where “ \top ” denotes transposition and \mathbf{r}^k is a $V \times 1$ vector containing the radii r_j^k of the k th prism. Let $\mathbf{d}(\mathbf{p})$ be the predicted data vector, whose i th element

$$d_i(\mathbf{p}) \equiv \sum_{k=1}^L f_i^k(\mathbf{r}^k, x_0^k, y_0^k, dz, z_1^k, m_0), \quad i = 1, \dots, N, \quad (2)$$

is the total-field anomaly produced by the ensemble of L prisms at the i th observation point (x_i, y_i, z_i) . In eq. 2, $f_i^k(\mathbf{r}^k, x_0^k, y_0^k, dz, z_1^k, m_0)$ is the total-field anomaly produced, at the observation point (x_i, y_i, z_i) , by the k th prism, with depth to the top $z_1^k = z_0 + (k - 1)dz$. We calculate $d_i(\mathbf{p})$ (eq. 2) by using the Python package Fatiando a Terra (Uieda et al. 2013), which implements the formulas proposed by Plouff (1976).

1.2 Inverse problem formulation

Given a set of tentative values for depth to the top of the shallowest prism z_0 and for the intensity of the total-magnetization of the source m_0 , we solve a constrained non-linear problem to estimate the parameter vector \mathbf{p} (eq. 1) by minimizing the objective function

$$\Gamma(\mathbf{p}) = \phi(\mathbf{p}) + \sum_{\ell=1}^7 \alpha_\ell \varphi_\ell(\mathbf{p}), \quad (3)$$

subject to

$$p_l^{min} < p_l < p_l^{max}, \quad l = 1, \dots, M, \quad (4)$$

where $\varphi(\mathbf{p})$ is the data-misfit function given by

$$\phi(\mathbf{p}) = \frac{1}{N} \|\mathbf{d}^o - \mathbf{d}(\mathbf{p})\|_2^2, \quad (5)$$

which represents the normalized squared Euclidean norm of the difference between the observed data vector \mathbf{d}^o and the predicted data vector $\mathbf{d}(\mathbf{p})$, α_ℓ is a positive number representing the weight of the ℓ th constraint function $\varphi_\ell(\mathbf{p})$ and p_l^{min} and p_l^{max} are, respectively, the lower and upper limits for the l th element p_l of the parameter vector \mathbf{p} (eq. 1). These limits are defined by the interpreter based on both the horizontal extent of the magnetic anomaly and the knowledge about the source. We use the Levenberg–Marquardt method (Aster et al. 2019, p. 240) to minimize the objective function $\Gamma(\mathbf{p})$ (equation 3) and introduce the inequality constraints (equation 4) by using a strategy similar to that presented by Barbosa et al. (1999).

1.3 Computational procedures

The regularization constraints depend on the weights $\tilde{\alpha}_\ell$ which are set by the interpret based on the prior information about the source. We set the vector $\tilde{\alpha}$ that contains each constraint weight to stabilize the inverse problem. The linear system solved by this method is given by

$$\Delta \hat{\mathbf{p}}_k^\dagger = \mathbf{D}_k \left(\mathbf{D}_k \mathbf{H}_k^\dagger \mathbf{D}_k + \lambda_k \mathbf{I} \right)^{-1} \mathbf{D}_k \mathbf{J}_k \quad (6)$$

The proposed methodology was implemented using the Marquardt's method:

- (i) Iteration $k = 0$: input \mathbf{d}^o , \mathbf{r} , z_0 , dz , \mathbf{p}^{min} , \mathbf{p}^{max} , α , and an initial approximation \mathbf{p}_0 satisfying the inequality constraints (equation 4);
- (ii) Obtain $\hat{\mathbf{p}}_k = f(\mathbf{p}_k)$ using the strategy proposed by Barbosa et al. (1999);
- (iii) Obtain $\Delta \hat{\mathbf{p}}_k^\dagger$ at the k th iteration by solving equation 3 using Marquardt's method;
- (iv) Compute: $\hat{\mathbf{p}}_{k+1}^\dagger = \hat{\mathbf{p}}_k^\dagger + \Delta \hat{\mathbf{p}}_k^\dagger$;
- (v) Obtain \mathbf{p}_{k+1}^\dagger using the inverse inequality function Barbosa et al. (1999);
- (vi) Test for algorithm convergence. Evaluate $|\Gamma(\hat{\mathbf{p}}_{k+1}) - \Gamma(\hat{\mathbf{p}}_k)|$.

where $\Gamma(\mathbf{p}^{k+1})$ and $\Gamma(\mathbf{p}^k)$ are the goal function (equation 3) evaluated at the iteration $k + 1$ and k , respectively.

1.4 Constraint functions

We have divided the constraint functions $\varphi_\ell(\mathbf{p})$ (eq. 3), $\ell = 1, \dots, 7$, used here to obtain stable solutions and introduce a priori information about the magnetic source into three groups.

1.4.1 Smoothness constraints

This group is formed by variations of the first-order Tikhonov regularization (Aster et al. 2019, p. 103) and impose smoothness on the radii r_j^k and the Cartesian coordinates x_0^k and y_0^k of the origin O^k , $j = 1, \dots, V$, $k = 1, \dots, L$, defining the horizontal section of each prism (Fig. 1b). They were proposed by Oliveira Jr. et al. (2011) and Oliveira Jr. & Barbosa (2013) and play a very role in introducing a priori information about the shape of the source.

The first constraint of this group is the *Smoothness constraint on the adjacent radii defining the horizontal section of each vertical prism*. This constraint imposes that adjacent radii r_j^k and r_{j+1}^k within each prism must be close to each other. It forces the estimated prism to be approximately cylindrical. We have conveniently rewritten this constraint in matrix form as follows:

$$\varphi_1(\mathbf{p}) = \mathbf{p}^\top \mathbf{R}_1^\top \mathbf{R}_1 \mathbf{p}, \quad (7)$$

where

$$\mathbf{R}_1 = \begin{bmatrix} \mathbf{S}_1 & \mathbf{0}_{LV \times 1} \end{bmatrix}_{LV \times M}, \quad (8)$$

$$\mathbf{S}_1 = \mathbf{I}_L \otimes \begin{bmatrix} (\mathbf{I}_V - \mathbf{D}_V^\top) & \mathbf{0}_{V \times 2} \end{bmatrix}, \quad (9)$$

$\mathbf{0}_{LV \times 1}$ is an $LV \times 1$ vector with null elements, \mathbf{I}_L is the identity matrix of order L , “ \otimes ” denotes the Kronecker product (Horn & Johnson 1991, p. 243), $\mathbf{0}_{V \times 2}$ is a $V \times 2$ matrix with null elements, \mathbf{I}_V is the identity matrix of order V and \mathbf{D}_V^\top is the upshift permutation matrix of order V (Golub & Loan 2013, p. 20).

The second constraint of this group is the *Smoothness constraint on the adjacent radii of the vertically adjacent prisms*, which imposes that adjacent radii r_j^k and r_{j+1}^{k+1} within vertically adjacent prisms must be close to each other. This constraint forces the shape of all prisms to be similar to each other and is given by

$$\varphi_2(\mathbf{p}) = \mathbf{p}^\top \mathbf{R}_2^\top \mathbf{R}_2 \mathbf{p}, \quad (10)$$

where

$$\mathbf{R}_2 = \begin{bmatrix} \mathbf{S}_2 & \mathbf{0}_{(L-1)V \times 1} \end{bmatrix}_{(L-1)V \times M}, \quad (11)$$

$$\mathbf{S}_2 = \left(\begin{bmatrix} \mathbf{I}_{L-1} & \mathbf{0}_{(L-1) \times 1} \end{bmatrix} - \begin{bmatrix} \mathbf{0}_{(L-1) \times 1} & \mathbf{I}_{L-1} \end{bmatrix} \right) \otimes \begin{bmatrix} \mathbf{I}_V & \mathbf{0}_{V \times 2} \end{bmatrix}, \quad (12)$$

$\mathbf{0}_{(L-1)V \times 1}$ is an $(L-1)V \times 1$ vector with null elements, $\mathbf{0}_{(L-1) \times 1}$ is an $(L-1) \times 1$ vector with null elements and \mathbf{I}_{L-1} is the identity matrix of order $L-1$.

The last constraint of this group is the *Smoothness constraint on the horizontal position of the arbitrary origins of the vertically adjacent prisms*. This constraint imposes that the estimated horizontal Cartesian coordinates (x_0^k, y_0^k) and (x_0^{k+1}, y_0^{k+1}) of the origins O^k and O^{k+1} of adjacent prisms must be close to each other. It forces the prisms to be vertically aligned. This constraint is given by

$$\varphi_3(\mathbf{p}) = \mathbf{p}^\top \mathbf{R}_3^\top \mathbf{R}_3 \mathbf{p} , \quad (13)$$

where

$$\mathbf{R}_3 = \begin{bmatrix} \mathbf{S}_3 & \mathbf{0}_{(L-1)2 \times 1} \end{bmatrix}_{(L-1)2 \times M} , \quad (14)$$

$$\mathbf{S}_3 = \left(\begin{bmatrix} \mathbf{I}_{L-1} & \mathbf{0}_{(L-1) \times 1} \end{bmatrix} - \begin{bmatrix} \mathbf{0}_{(L-1) \times 1} & \mathbf{I}_{L-1} \end{bmatrix} \right) \otimes \begin{bmatrix} \mathbf{0}_{2 \times V} & \mathbf{I}_2 \end{bmatrix} , \quad (15)$$

$\mathbf{0}_{(L-1)2 \times 1}$ is an $(L-1)2 \times 1$ vector with null elements, $\mathbf{0}_{2 \times V}$ is a $2 \times V$ matrix with null elements and \mathbf{I}_2 is the identity matrix of order 2.

1.4.2 Equality constraints

This group is formed by two constraints that were proposed by Oliveira Jr. et al. (2011) and Oliveira Jr. & Barbosa (2013) by following the same approach proposed Barbosa et al. (1997) and Barbosa et al. (1999). They introduce a priori information about the shallowest prism and are suitable for outcropping sources.

The *Source's outcrop constraint* imposes that the horizontal cross-section of the shallowest prism must be close to the intersection of the geologic source with the known outcropping boundary. The matrix form of this constraint is given by

$$\varphi_4(\mathbf{p}) = (\mathbf{R}_4 \mathbf{p} - \mathbf{a})^\top (\mathbf{R}_4 \mathbf{p} - \mathbf{a}) , \quad (16)$$

where \mathbf{a} is a vector containing the radii and the horizontal Cartesian coordinates of the polygon defining the outcropping boundary

$$\mathbf{a} = \begin{bmatrix} \tilde{r}_1^0 & \dots & \tilde{r}_V^0 & \tilde{x}_0^0 & \tilde{y}_0^0 \end{bmatrix}^\top , \quad (17)$$

and

$$\mathbf{R}_4 = \begin{bmatrix} \mathbf{I}_{V+2} & \mathbf{0}_{(V+2) \times (M-V-2)} \end{bmatrix}_{(V+2) \times M} , \quad (18)$$

where \mathbf{I}_{V+2} is the identity matrix of order $V+2$ and $\mathbf{0}_{(V+2) \times (M-V-2)}$ is a matrix with null elements.

The *Source's horizontal location constraint* imposes that the horizontal Cartesian coordinates of the origin within the shallowest prism must be as close as possible to a known outcropping point. The

matrix form of the this constraint is given by

$$\varphi_5(\mathbf{p}) = (\mathbf{R}_5\mathbf{p} - \mathbf{b})^\top (\mathbf{R}_5\mathbf{p} - \mathbf{b}) , \quad (19)$$

where \mathbf{b} is a vector containing the horizontal Cartesian coordinates of the outcropping point

$$\mathbf{b} = \begin{bmatrix} \hat{x}_0^0 & \hat{y}_0^0 \end{bmatrix}^\top , \quad (20)$$

and

$$\mathbf{R}_5 = \begin{bmatrix} \mathbf{0}_{2 \times V} & \mathbf{I}_2 & \mathbf{0}_{2 \times (M-V-2)} \end{bmatrix}_{2 \times M} , \quad (21)$$

where \mathbf{I}_2 is the identity matrix of order 2 and $\mathbf{0}_{2 \times (M-V-2)}$ and $\mathbf{0}_{2 \times V}$ are matrices with null elements.

1.4.3 Minimum Euclidean norm constraints

Two constraints use the zeroth-order Tikhonov regularization with the purpose of obtaining stable solutions without necessarily introducing significant a priori information about the source.

The *Minimum Euclidean norm of the radii* imposes that all estimated radii within each prism must be close to null values. This constraint were proposed by Oliveira Jr. et al. (2011) and Oliveira Jr. & Barbosa (2013) and can be rewritten in matrix form as follows

$$\varphi_6(\mathbf{p}) = \mathbf{p}^\top \mathbf{R}_6^\top \mathbf{R}_6 \mathbf{p} , \quad (22)$$

where

$$\mathbf{R}_6 = \begin{bmatrix} \mathbf{S}_6 & \mathbf{0}_{(M-1) \times 1} \\ \mathbf{0}_{1 \times (M-1)} & 0 \end{bmatrix}_{M \times M} , \quad (23)$$

and

$$\mathbf{S}_6 = \begin{bmatrix} \mathbf{I}_V & \mathbf{0}_{V \times 2} \\ \mathbf{0}_{2 \times V} & \mathbf{I}_2 \end{bmatrix}_{(V+2) \times (V+2)} . \quad (24)$$

The other constraint, the *Minimum Euclidean norm of the thickness*, imposes that the thickness of all prisms must be close to zero. This constraint were developed here to introduce a priori information about the maximum depth of the source. Its matrix form is given by

$$\varphi_7 = \mathbf{p}^\top \mathbf{R}_7^\top \mathbf{R}_7 \mathbf{p} , \quad (25)$$

where

$$\mathbf{R}_7 = \begin{bmatrix} \mathbf{0}_{(M-1) \times (M-1)} & \mathbf{0}_{(M-1) \times 1} \\ \mathbf{0}_{1 \times (M-1)} & 1 \end{bmatrix}_{M \times M} . \quad (26)$$

2 APPLICATION TO SYNTHETIC DATA

To examine the performance of our inversion method, we present two applications with total-field anomaly data simulating two different isolated geological sources. The first source is a funnel-shaped model with a simple geometry, which satisfies all of the constraints described in Section 1. The aim of this test is to evaluate the regularization in an ideal case with simple geometry. The second source has a complex geometry, which does not satisfy any constraint. The purpose, here, is to show that the constraints can stabilize the inverse problem in a more realistic case retrieving the geometry of the source with known magnetization using the polygonal prisms.

In both applications, the synthetic total-field anomaly was computed in an irregular grid on plane $z = -150$ m and contaminated with pseudo-random Gaussian noise sequences with mean zero and different standard deviation. In both cases, we considered the main magnetic field with an inclination and declination of -21.5° and -18.7° , respectively. Also, the total-magnetization direction of the models is the same with a strong remnant component of $(-50^\circ, 9^\circ)$ for inclination and declination, respectively.

Although the simulated sources have a different depth to the top, we have considered both known. We also assumed the same magnetization for all prisms of the magnetic sources. On the other hand, the depth extent of the sources was not set in the initial guesses because it is a parameter for the inverse problem. Moreover, we have investigated the influence of the parameters from the initial guess on the solution by varying them and evaluating the effect on the misfit function.

2.1 Simple model test

The first synthetic source has $L = 8$ prisms, each one with $M = 20$ vertices, and a purely induced magnetization with an intensity of 9 A/m. Its depth to the top is at $z_0 = 0$ m and the bottom is at 1600 m. The radii of the vertices are equal within the same prism and decrease along the depth with a step of 160 m starting with $r_j^k = 1920$ m, $j = 1, \dots, M$ (Figure 3b). The horizontal coordinates x_0 and y_0 of the origins of the polygons O^k are equal to $(0, 0)$ for all prisms. We calculated the synthetic data produced by this source on an area of 100 km^2 , simulating an airborne survey composed of 20 flight lines that are equally spaced with 500 m between them along the horizontal coordinate y , at a constant vertical coordinate $z = -150$ m (Figure 3a).

For the inversion, we used an interpretation model formed by $L = 5$ prisms, each one with $M = 20$ vertices. The prisms forming the initial approximation have the same radii for all vertices (2000 m) and depth extent (350 m), so the maximum depth is equal to 1750 m. We have used all constraints described in Section 2 except the third and fourth constraints. We weighted the constraints with $\alpha_1 = 10^{-4}$, $\alpha_2 = 10^{-4}$, $\alpha_5 = 10^{-4}$, $\alpha_6 = 10^{-6}$, and $\alpha_7 = 10^{-4}$. Both Cartesian coordinates x_0^k and y_0^k

of the origins of all prisms O^k , $k = 1, \dots, L$, are located at the point $(0, 0)$ of the area. Fig. 5c and d show the result of the inversion of the noise-corrupted total-field anomaly in Fig. 5a. The red prisms are very close to the edges of the true body (blue lines) even using fewer prisms than the true body has. Moreover, the estimated depth extent of each prism is $dz = 200.65$ m, which gives us a very accurate total depth extent of 1203.88 m. Figure 5a shows that the residuals have a mean very close to zero ($\mu = 0.09$ nT) and a coherent standard deviation ($\sigma = 5.23$ nT).

2.2 Complex model test

The second synthetic source has $L = 10$ prisms, each one with $M = 30$ vertices, and a total magnetization with intensity $\|\mathbf{m}\| = 10$ A/m. The complex model has both induced and remnant magnetization with inclination 65° , and declination -40.5° . Its depth to the top z_0 is 200 m and its bottom is at 4200 m. The radii of the vertices $(r_j^k, j = 1, \dots, M, k = 1, \dots, L)$ forming this synthetic body vary from 240 to 1540 m and the horizontal coordinates x_0 and y_0 of the origins of the polygons O^k vary from -250 m and 250 m to 750 m and -750 m, respectively (Figure 6a) by an equal step for both of 100 m. We calculated the synthetic data produced by this body, simulating an airborne survey covering an area of 100 km^2 composed of 21 flight lines that are equally spaced from -5000 m to 5000 m, along with the horizontal coordinate y , and with a height of -100 m (Figure 6b). The initial guess is a cylinder formed by $L = 8$ prisms, each one with $M = 15$ vertices centered at $(x_0^k, y_0^k) = (0, 0)$. All prisms that form the initial approximation have the same radii (500 m) and depth extent (600 m) reaching 4800 m of maximum depth (Figure 6a).

We set the weights for the constraints $\alpha_1 = 0.0005$, $\alpha_2 = 0.003$, $\alpha_5 = 0.05$, $\alpha_6 = 0.00001$, and $\alpha_7 = 0.04$. Again, the third and fourth constraints were not used. Fig. 8a shows the result of the inversion of the noise-corrupted total-field anomaly in Fig. 6. Due to the lower number of prisms in the interpretation model, the estimated body does not retrieve perfectly the simulated body. However, the volume of the complex model is 8.40 km^3 , while the volume of the estimated source is 8.29 km^3 . Moreover, the estimated depth extent is 3875.4 m, which is close to 4000 m. The residuals have a mean and a standard deviation very close to the values of the noise also the histogram is coherent with a Gaussian distribution (Figure 8d).

ACKNOWLEDGMENTS

REFERENCES

- Aster, R. C., Borchers, B., & Thurber, C. H., 2019. *Parameter Estimation and Inverse Problems*, Elsevier, 3rd edn.
- Barbosa, V. C. F., Silva, J. B. C., & Medeiros, W. E., 1997. Gravity inversion of basement relief using approximate equality constraints on depths, *Geophysics*, **62**, 1745–1757.
- Barbosa, V. C. F., Silva, J. B. C., & Medeiros, W. E., 1999. Gravity inversion of a discontinuous relief stabilized by weighted smoothness constraints on depth, *Geophysics*, **64**(5), 1429–1437.
- Golub, G. H. & Loan, C. F. V., 2013. *Matrix Computations (Johns Hopkins Studies in the Mathematical Sciences)*, Johns Hopkins University Press, 4th edn.
- Horn, R. A. & Johnson, C. R., 1991. *Topics in Matrix Analysis*, Cambridge University Press, 1st edn.
- Oliveira Jr., V. C. & Barbosa, V. C. F., 2013. 3-D radial gravity gradient inversion, *Geophysical Journal International*, **195**(2), 883–902.
- Oliveira Jr., V. C., Barbosa, V. C. F., & Silva, J. B. C., 2011. Source geometry estimation using the mass excess criterion to constrain 3-D radial inversion of gravity data, *Geophysical Journal International*, **187**(2), 754–772.
- Plouff, D., 1976. Gravity and magnetic fields of polygonal prisms and application to magnetic terrain corrections, *Geophysics*, **41**(4), 727–741.
- Uieda, L., Oliveira Jr., V. C., & Barbosa, V. C. F., 2013. Modeling the earth with fatiando a terra, in *Proceedings of the 12th Python in Science Conference*, pp. 96 – 103.

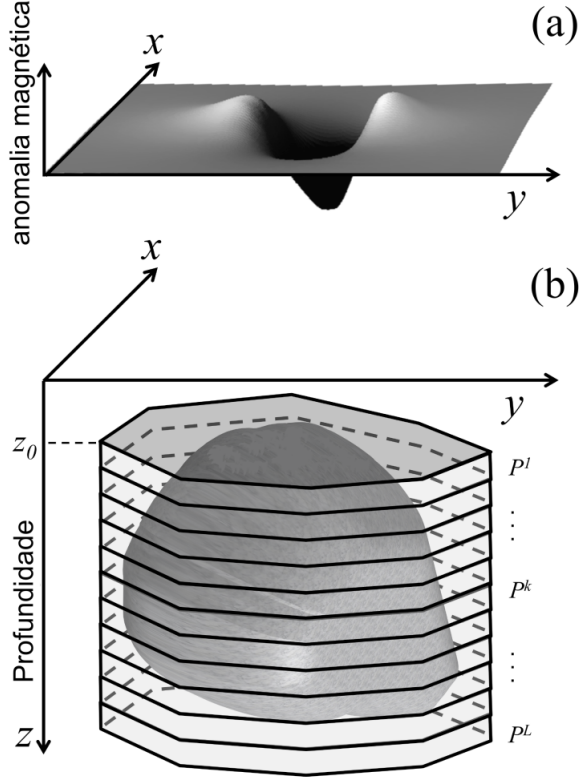


Figure 1. Schematic representation of (a) total-field anomaly (gray surface) produced by (b) a 3-D anomalous source (dark gray volume). The interpretation model in (b) consists of a set of L vertical, juxtaposed 3-D prisms P^k , $k = 1, \dots, L$, (light gray prisms) in the vertical direction of a right-handed coordinate system.

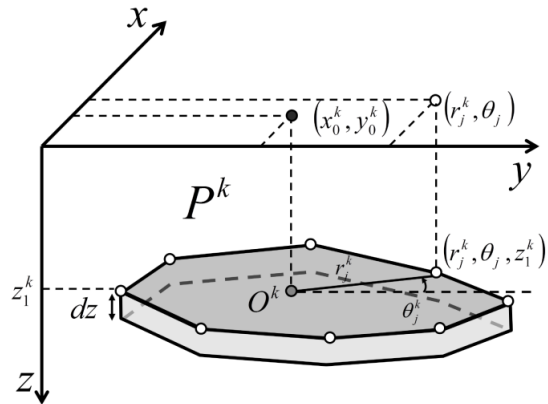


Figure 2. Polygonal cross-section of the k th vertical prism P^k described by V vertices (white dots) with polar coordinates (r_j^k, θ_j^k) , $j = 1, \dots, V$, $k = 1, \dots, L$, referred to an arbitrary origin O^k (grey dot) with horizontal Cartesian coordinates (x_0^k, y_0^k) , $k = 1, \dots, L$.

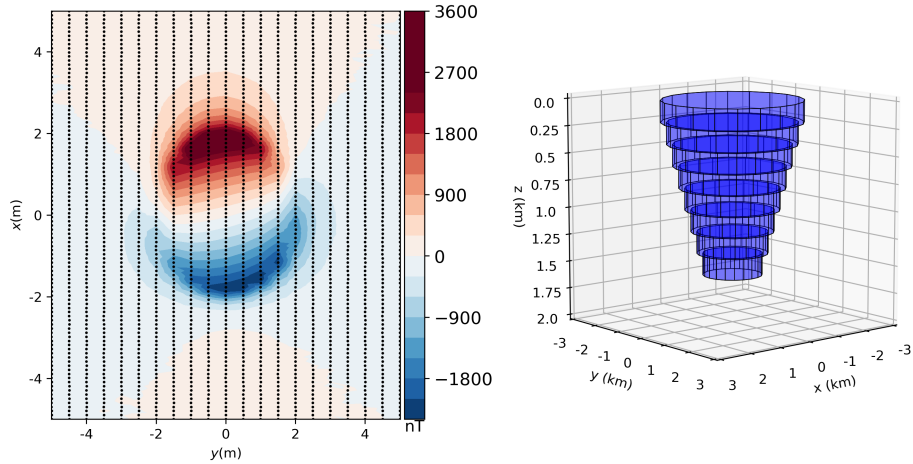


Figure 3. Simple model simulation. (a) noise-corrupted total-field anomaly produced by the simple model (blue prisms) in (b). The black dots represent the observation points that simulate an airborne survey.

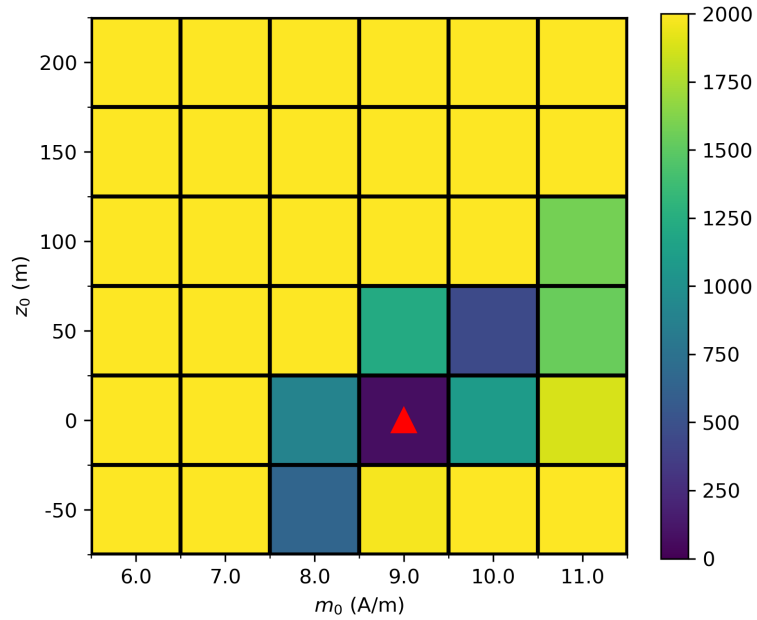


Figure 4. Map of the objective function values due to the inverse solutions for the simple model. Each square is a value of the objective function of a solution of the inverse problem for a pair of the total-magnetization intensity and the depth to the top of the source. The red triangle represents the true values for m_0 and z_0 .

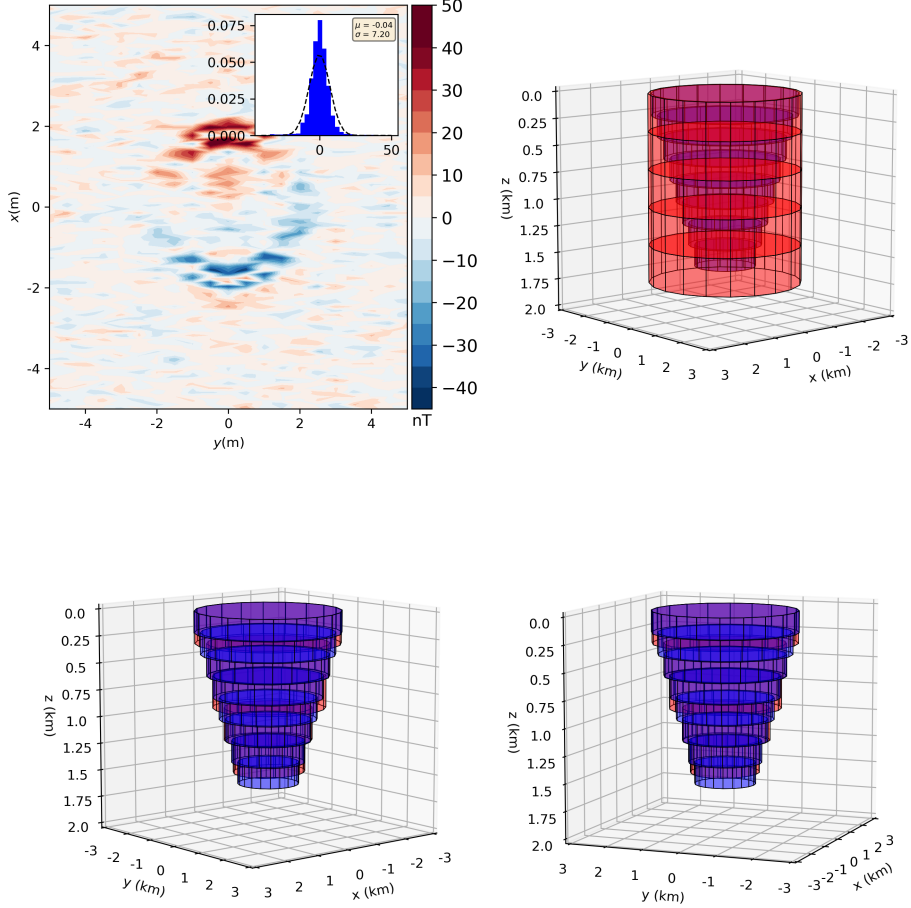


Figure 5. Application to simple model data. (a) residual data given by the difference between the noise-corrupted data (Fig. 3(a)) and the predicted data (not shown) produced by the inverse model (red prisms) in (c) and (d). These inversions were computed using the same cylinder as a initial approximation. The red prisms in (b) represent the input model of the inversion.

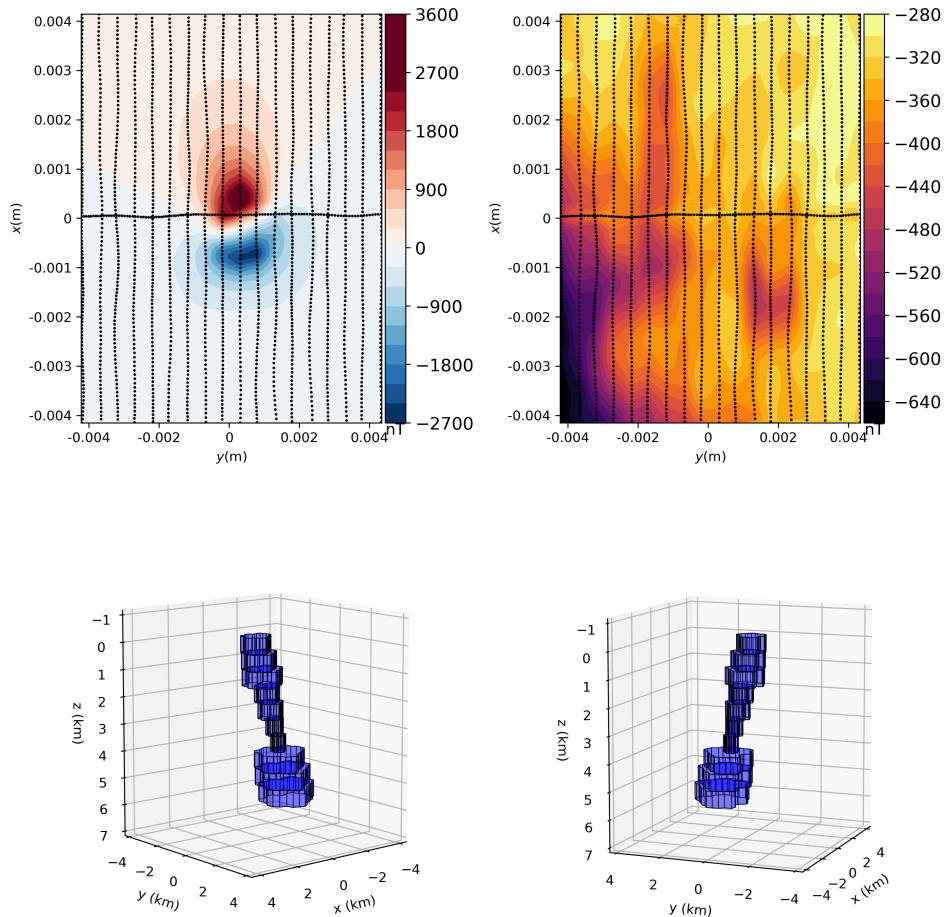


Figure 6. Complex model simulation. (a) noise-corrupted total-field anomaly produced by the complex model (blue prisms) in (c) and (d). The black dots represent the observation points that simulate an airborne survey.

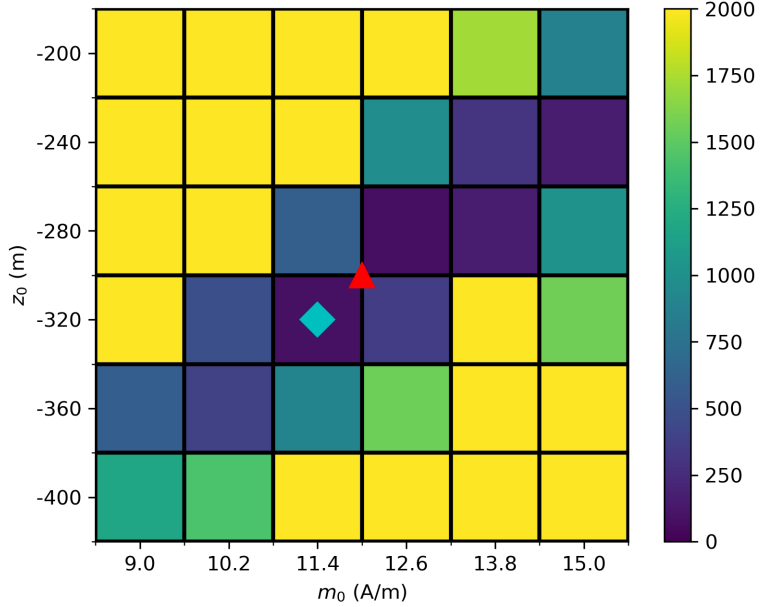


Figure 7. Map of the objective function values due to the inverse solutions for the complex model. Each square is a value of the objective function of a solution of the inverse problem for a pair of the total-magnetization intensity and the depth to the top of the source. These inversions were computed using the same cylinder as a initial approximation. The red triangle represents the true values for m_0 and z_0 . The cyan diamond represents the solution with the lowest function value.

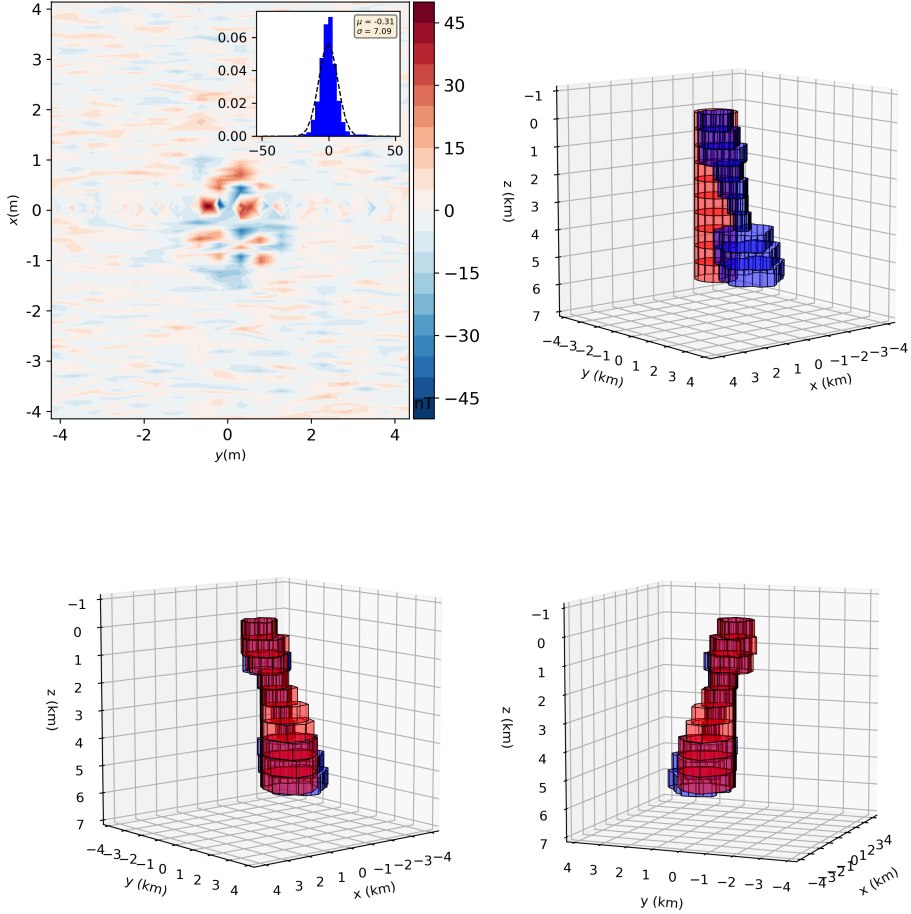


Figure 8. Application to complex model data. (a) residual data given by the difference between the noise-corrupted data (Fig. 6(a)) and the predicted data (not shown) produced by the inverse model (red prisms) in (c) and (d). The red prisms in (b) represent the input model of the inversion.

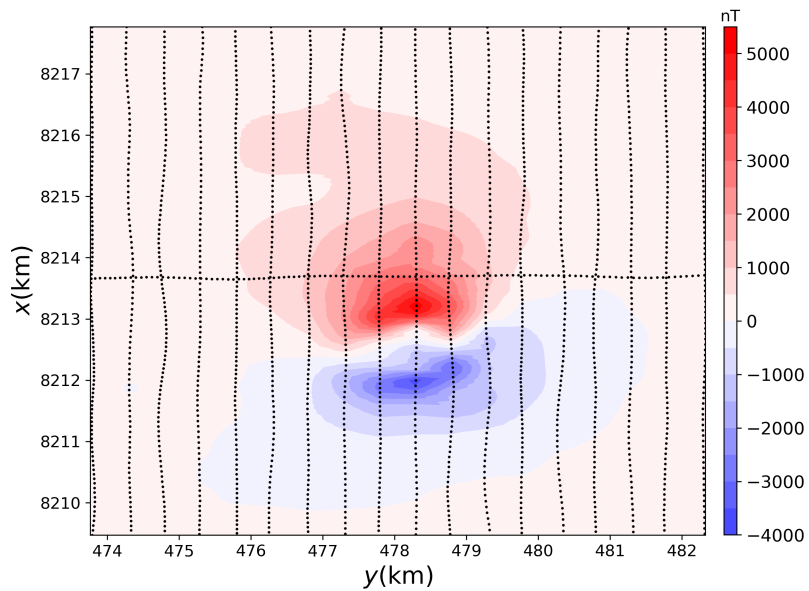


Figure 9. Total-field anomaly of Diorama in GAP. The black dots are the observation points used in this work.

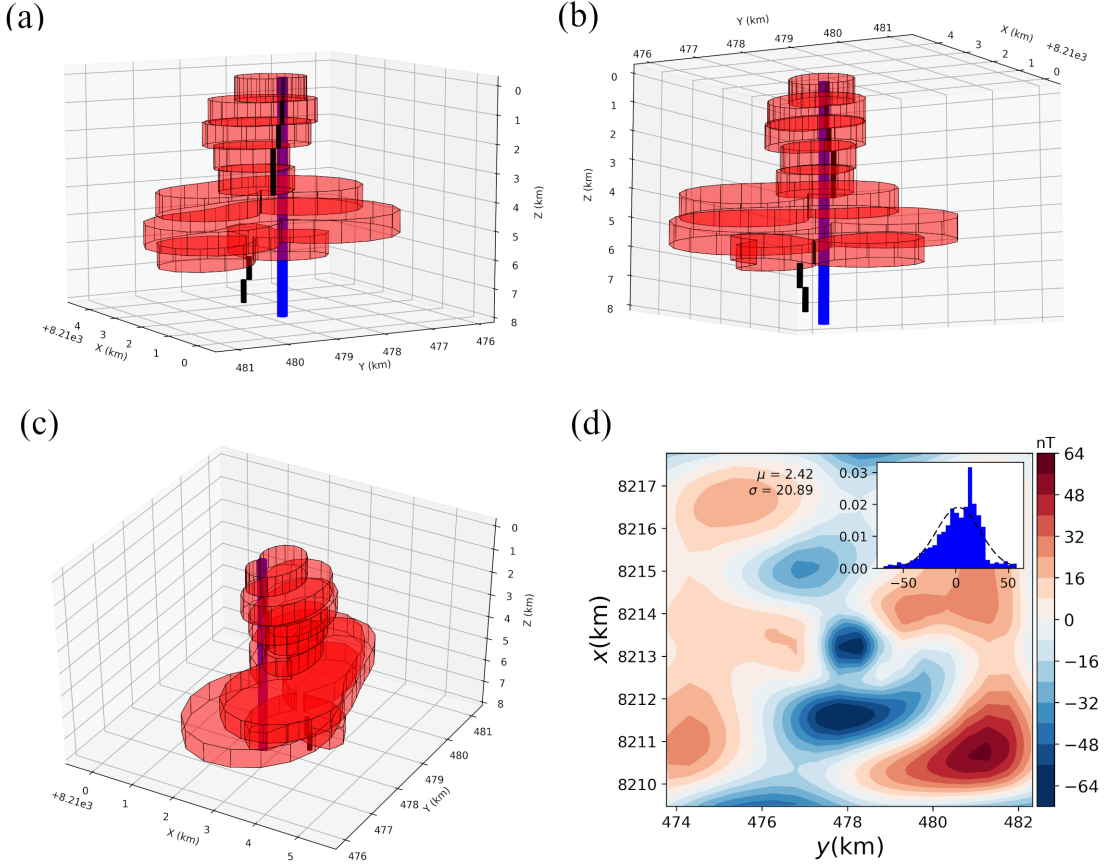


Figure 10. Perspective views of the initial guess (blue cylinder) and the estimated source (red prisms) in (a), (b) and (c). (d) Residuals defined as the difference between the noisy and the predicted (not shown) total-field anomalies and the histogram of the residuals (inset in d) with mean $\mu = 2.42$ nT and standard deviation $\sigma = 20.89$ nT. The dashed line on the inset is the Gaussian curve for the residuals.